Mathematical Biosciences and Engineering, 16(4): 2959–2972.
DOI: 10.3934/mbe.2019146
Received: 24 December 2018
Accepted: 12 March 2019
Published: 10 April 2019

http://www.aimspress.com/journal/MBE

Research article

Comparative anatomy of the mouse and human ankle joint using Micro-CT: Utility of a mouse model to study human ankle sprains

Chao Gao[1,2,#], Zhi Chen[1,2,#], Yu Cheng[1,2,#], Junkun Li1[2], Xiaowei Huang[2], Liangyi Wei[1,2], FanHe[1], Zong-ping Luo[1], Hongtao Zhang[2,*]and Jia Yu[1,*]

[1] Orthopedic Institute, Medical College, Soochow University, Suzhou, China
[2] Department of Orthopedics, The First Affiliated Hospital of Soochow University, Suzhou, China

*** Correspondence:** Email: htzhangsz@163.com; jiayu@suda.edu.cn.

[#] These authors contributed equally to this study.

Abstract: The use of mouse models as a tool to study ankle sprain requires a basic understanding of the similarities and differences between human and mouse ankle joint anatomy. However, few studies have been conducted that address the merits and drawbacks of these differences in the functioning of joints. Twenty hindfoot specimens were obtained from 10 male C57BL/6J mice and scanned using micro-CT. The foot and ankle skeletal structures were reconstructed in three dimensions. Morphological parameters were then measured using a plane projection method and normalized data were compared with those of human ankles. There was no significant difference in the malleolar width, maximal tibial thickness, tibial arc length, trochlea tali arc length or trochlea tali width of the mouse specimens compared with the human model. However, a groove was observed on the talar dome in the mouse specimens which was not observed in humans, the talar dome being more symmetric. The mouse ankle was to a large extent able to mimic the mechanism of a human ankle and so a mouse model could be appropriate for expanding our understanding of ankle biomechanics in general. However, the structural differences in the talar dome in the mouse and human should not be ignored. Although there are some differences in the mouse and human ankle that cannot be ignored, compared to other animals, the human ankle is more similar to that of the mouse.

Keywords: talocrural joint; musculoskeletal anatomy; talar dome; rodent; foot biomechanics

1. Introduction

Foot and ankle injuries are amongst the most common encountered during daily life and sports activities [1]. In the United States, foot and ankle injury account for more than three million emergency department visits annually [2]. Of these, ankle sprain contributes a large proportion with an overall incidence of 2.15 per 1000 persons [3]. Suitable and comprehensive research models of ankle sprain should be utilized to explore the mechanisms of injury and the effectiveness of different treatment paradigms. Previous studies have attempted to employ cadaveric models [4] and computer simulations to identify injury mechanisms but these have been inconclusive [5–7]. Researchers have developed animal models to answer biomechanical questions since they have many advantages over alternative approaches [3,8–10]. Icro surgical techniques, other novel assessment tools including histological investigation and gait analysis could be employed to analyze ankle sprain and cartilage injury [11]. Of a number of animal models, such as the chimpanzee, cow, dog, rabbit and mouse (Figure 1), only mice and rats were found to have a suitable plantigrade joint and kinematics that had gross similarity with those of a human. Although rabbits and chimpanzees are plantigrade species, rabbits are sedentary because of their human-designed housing, and chimpanzees are too expensive for this study, and have thus mice been recognized as key animal models to study the mechanism of ankle injury [11–13].

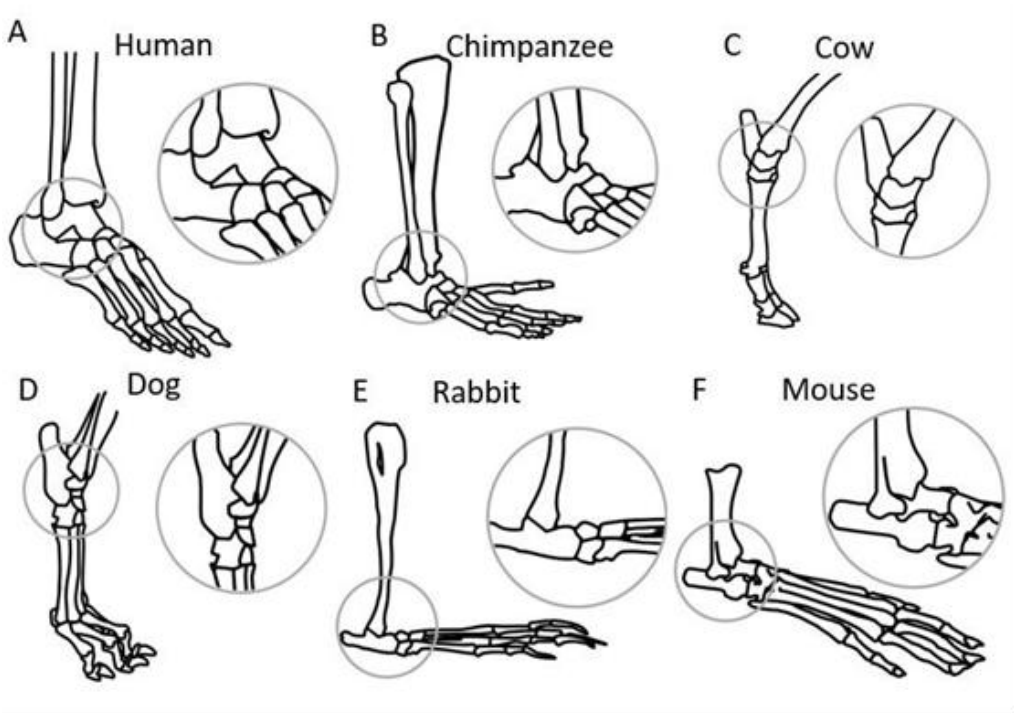

Figure 1. Foot and ankle skeletal structures of different species with enlarged ankle detail: A. Human, B. Chimpanzee, C. Cow, D. Dog, E. Rabbit, F. Mouse.

Researchers attempts to establish a sprained ankle instability model using either a mouse or rat [13] resulted in such a model being established in the rat for the first time by accurately cutting the lateral ligament of the ankle joint. Following this principle, Hubbard-Turner and his team established in 2013 [11] and in 2015 [14] acute and chronic ankle instability mouse models. Based on behavioral test comparisons, they found that different severities of ligament injury had a significant impact on the ability of an animal to balance, and their model demonstrated good reproducibility. In 2015, Chang et al. [12] used a similar mouse model of ankle instability, and used micro-CT scanning and comparisons of mouse and humans using immunohistochemistry of ankle joint structures and the cartilage thickness ratio. The results demonstrated that the gross anatomical structure of the ankle joint and cartilaginous tissue is very similar. Previous researchers also induced atrophy of the peroneus longus (PL) and peroneus brevis (PB) muscles to examine the progression of clubfoot disease [15]and used gait analysis of a mouse following ligation of the common peroneal nerve [16].

However, up to now, no comprehensive comparative study pinpointing the similarities and differences in the skeletal anatomy between the human and mouse ankle has been published. The anatomical structure determines its function. The similarity in three-dimensional structures is not concrete proof that supports the reliability of animal models. In this study, we hypothesized that the mouse ankle joint could be closely analogous to the human ankle joint at the skeletal level.

X-rays have been used for many years to perform two-dimensional (2D) anatomical measurements [17,18], but because of the influence of the precise positioning of the complex morphology, measurements based on such X-rays cannot render a true three-dimensional (3D) representation and so the results are generally inconsistent. More accurate data can be obtained from images from CT scanning [15,19,20]. To better understand the mouse ankle joint, an animal model can be established that allows reconstruction of a 3D model from CT images and then using plane projection to compare its structure with that of a human from reference data obtained from previous measurements [21]. Structural variables such as length, width, radius and angle of ankle joint were thus compared to determine the differences in the study cohort.

2. Materials and method

2.1. Preparation of specimens

Ten 10-week-old male black C57BL/6J mice, weighing 25–27g, were purchased from the animal center of Soochow University. All experiments were approved by the Animal Research Ethics Committee of Soochow University. Mice were euthanized by cervical dislocation, and both hindlimbs one centimeter below the knee joint were removed, skinned and immediately, affixed to 3D-printed plastic frames (Figure 2A) All frames were 3D-printed in nylon using selective laser sintering (SLS). In total 20hindfoot specimens were scanned in the neutral position, with six randomly selected to be scanned at both 30 °plantarflexion and 30 °dorsiflexion. During micro-CT scanning, each specimen was positioned on the frames according to a previously published procedure. The base-plate of the frame used for the neutral position (0 °) was 30 mm in length, 8 mm in width and 3 mm in thickness and the vertical plate was 30 mm in length, 15 mm wide and 3 mm thick. The frames used for dorsiflexion and plantarflexion scanning had similar designs but with different flexion angles. Each mouse foot was fixed to its base-plate with adhesive tape with

the long axis of the base-plate aligned with a line connecting the calcaneal insertion of the Achilles tendon and the third metatarsal head. The lower limb was aligned to the long axis of the vertical plate (Figure 2B). After fixation, the specimen-frame construct was scanned with a micro-CT scanner (Sky scan 1176, Belgium) using the following parameters: 50 kV, 500 mA at a resolution of 18 μm. Each micro-CT image had dimensions of 1296 × 1296 pixels. Approximately 500 images were scanned for each specimen over a duration of 25 minutes.

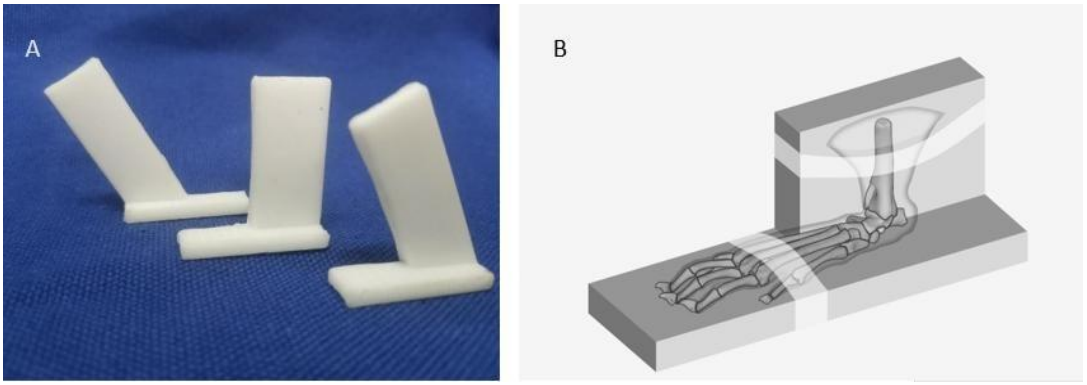

Figure 2. Frames for fixation of hindlimbs. A: 3D printed frames for fixation of the hindfoot of mice with three angles: neutral, 30 degrees plantarflexion and 30 degrees dorsiflexion. B: mouse hindfoot fixed on the 3D printed frame.

2.2. Micro-CT-based skeletal models and morphological parameters

A global coordinate system was defined for the ankle specimens to allow subsequent quantitative morphological descriptions. The anteroposterior(A/P) axis was defined as a line through the calcaneal insertion of the Achilles tendon and the head of the third metatarsal, which was parallel to the base-plate. The super inferior (S/I) axis was perpendicular to the base-plate. The mediolateral(M/L) axis was parallel to the base-plate, defined as a line perpendicular to both the (A/P) and (S/I) axes. For comparisons with human models, 13 morphological parameters in the tibia-fibula segments were defined with reference to a previous human ankle anatomy study of mostly Chinese people [21], and measurement of talar rotation around the vertical tibial axis at a plantarflexion or dorsiflexion angle of 30 °, also referencing a previous human study [22]. All bone models based on 2D and 3Dgeometrical parameter definitions are provided in Table 1 and Figure 3. The human model was redepicted from our previous study [23], with human reference data from the Kuo study in which CT was used to measure 20 humans [21]. The clinician who performed the measurements is an ankle surgeon with extensive experience in ankle anatomy. Prior to the formal experiment, he conducted repeated measurements on an ankle specimen, resulting in an intraclass correlation coefficient (ICC) = 0.8, indicating a high degree of confidence.

2.3. Definition of 2D and 3D morphological parameters

Medical image segmentation software (Mimics Innovation Suite v15.0, Materialize, Belgium) was used to measure and reconstruct the 3D mouse ankle models. 2Dmeasurements were made by projecting a silhouette of the 3D model onto different planes. The XY plane was defined as a

cross-section, the XZ plane as coronal and the YZ plane as sagittal. For example, MTiTH projected in the sagittal plane allowed measurement of its 2D length. MalW projected in the coronal plane measured its 2Dlength, while 3D morphological parameters including trochlea tali arc length (TaAL) and trochlea tali width (TaW) were directly measured on the 3D ankle models.

Table 1. Definitions of the Parameters Used to Describe the Morphology of the Distal Tibia and Talus from Kuo's paper. See also Figure 3 for relevant graphical descriptions.

	Definitions
Distal Tibia	
TiAL(mm)	Tibial arc length: distance between the most anterior (A) and posterior (B) points of the maximal arc of the tibial mortise in the sagittal plane
TiSR(mm)	Tibial sagittal radius: radius of the AB arc
APA (deg)	Anteroposterior inclination angle: inclination angle between the A/P axis and the AB segment
MTiTh(mm)	Maximal tibial thickness: The A/P distance from the most anterior to the most posterior point on the tibial profile in the sagittal plane
TiW(mm)	Tibial width: M/L distance of the tibial mortise calculated using the two end-points of the anterior (TiWa) and posterior (TiWp) edges
MaIW(mm)	Malleolar width: M/L distance between the most lateral point of the fibula and the most medial point of the tibia
MLATi(deg)	Angle in the frontal plane between the M/L axis and the line joining the most distal points of the fibula and tibia
Talus	
TaAL(mm)	Trochlea tali arc length: distance between the most anterior (A) and posterior (B) points of the trochlea tali, as seen in the sagittal projection of the talus. The suffixes m, l and c indicate the corresponding medial, lateral and central arcs separately
TaIA (deg)	Trochlea tali inclination angle: inclination angle in the transverse plane between the medial and lateral crest of the talar dome, identified by the AmPm and AlPl segments
TaW(a,p,c) (mm)	Trochlea tali width: width between medial and lateral crests of the talar dome. The suffix a, p and c indicates this width, respectively, in the most anterior, most posterior and central location along M/L axis
TaR(m,l,n) (mm)	Trochlea tali radius: radius of the talar dome in the sagittal plane, as identified by the arc GF. The suffixes m, l and n indicate the corresponding medial, lateral and narrowest arcs
TaHt (mm)	Talus height: height of the Talus head, calculated as the S/I distance between the top and bottom of the talus head (see also TaAL)
MLATa (deg)	Angle in the frontal plane between the M/L axis and the line joining the two most proximal vertices of the trochlea tali
TTVR (deg)	Talus-tibia vertical rotation: The rotation angle change of the talus around vertical tibia axis compared with foot neutral position in the transverse section (xy) plane, positive difference between values denotes internal rotation around the vertical axis

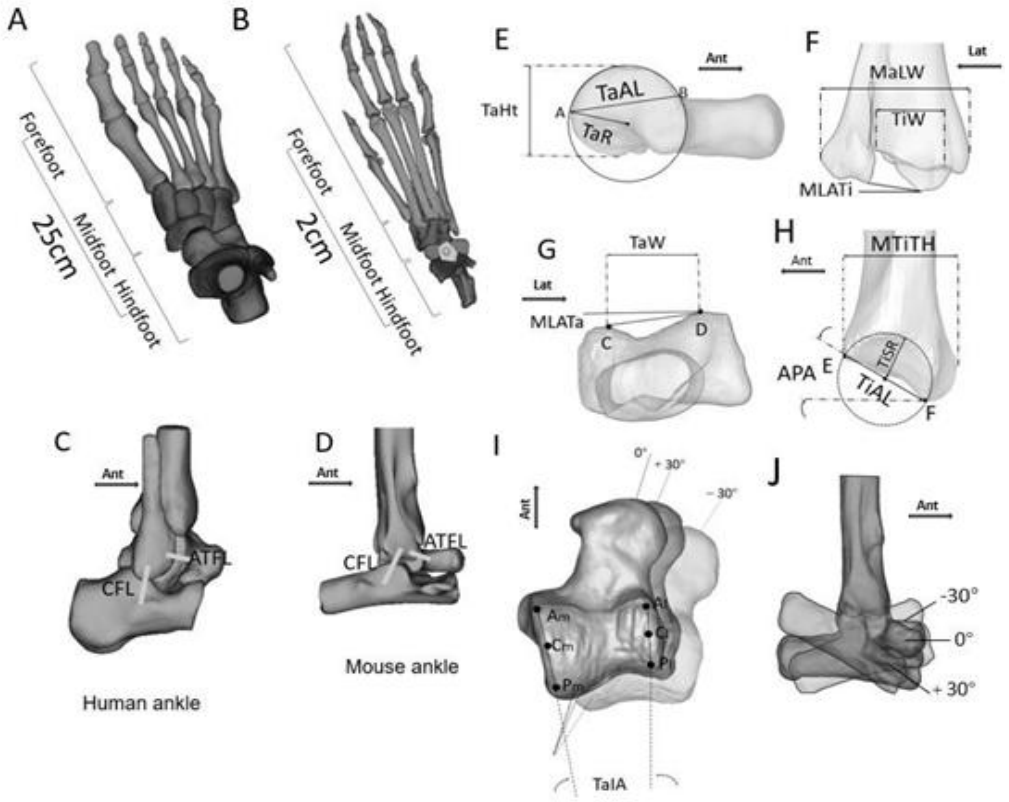

Figure 3. Graphical depiction of the parameters defined on the 3D skeletal models. In the transverse plane view (A: human foot and ankle, B: mouse foot and ankle, I: mouse talus), in the sagittal plane (C: human ankle with CFL (calcaneofibular ligament) and ATFL (anterior talofibular ligament), D: mouse ankle with CFL and ATFL, E: mouse talus, H: mouse tibia, J: mouse tibia and talus), in the frontal plane (F: mouse tibia and fibula, G: mouse talus). Definitions of each parameter are also provided in Table 1.

2.4. Normalized Data and Statistical Analysis

To compare the ankle size data of mice with those of humans, both sets required normalization. The thickness and width of the ankle joints and talar dome height were chosen as the reference measurement of the three planes for standardization. Thus, the ratio of MTiTH to MalW and that of mice to human samples were used for normalization on the sagittal, transverse and coronal planes, respectively. All statistical analyses were performed by independent t-tests using Sigma Plot 14.0 with a significance level set at $p = 0.05$.

3. Results

The means, standard deviations, 95% confidence intervals and p values of all morphological parameters of all specimens are summarized in Table 2. In the ankle joint, the morphological parameters, including malleolar width (MalW), maximal tibial thickness (MTiTH), tibial arc length (TaAL), trochlea tali arc length (TiAL) and the most anterior trochlea tali width (TaWa) of the mouse and human specimens were not significantly different ($p > 0.05$). The MTiTH

to MalW ratio of mice were 1.52 and that of the humans was 1.51 or 1.63, indicating they were morphologically similar (Figure 4). The ratio of malleolar width (MalW) to tibial width (TiW) in mouse and human data were 0.53 and 0.47, respectively. For comparisons of normalized mouse and human size data [21], the parameters TiSR, TaRl and TaRn were 45.8%,19.3% and 52.7% smaller in the mouse than in humans, respectively. However, TiW, TaW, TaWp and TaH were 12.6%, 30.8%，68.0% and22.5%larger in the mouse than in humans, respectively. A groove was found on the talar dome in the mouse but not in humans, the mouse trochlea tali radius (TaR) of the talar dome was at least 19.3% smaller than in humans and the lateral side of the arc radius was 36.6% larger than the medial side in the mouse while in humans they were almost the same size. In addition, MLATi and TaIA in the mouse were 6.62 and 8.82 °smaller than in the human, respectively. APA and MLATa in the mouse were 18.94and 6.96 ° larger than in the human, respectively. The mouse TiAL/TiW and TaAL/TaW ratios were 0.90 and 1.15, respectively, compared to mean values in the human of 0.87 and 1.55 [21], 1.01 and 1.37 [18], and 0.89 and 1.19 [17], respectively. The human model was redepicited from our previous study [23], with human reference data from the Kuo study in which CT was used to measure 20 humans [21]. (Figures 5 and 6). The rotation of the talus around the vertical tibial axis was measured at 30 ° dorsiflexion and plantarflexion and compared with the neutral position for each specimen (Figure 7). The TTVR was −4.89 ° and −11.49 ° for dorsiflexion and plantarflexion, respectively.

Table 2. Means and standard deviations of the normalized mouse data compared to those for humans for morphological parameters of the ankle joint.

		Mouse	Human	
	Parameters	Normalized data	KUO et al(2014)	
		(n = 20)	(n = 58)	
		Mean ± SD	Mean ± SD	P-value
Tibia	TiAL	28.12 ± 2.65	28.4 ± 2.9	0.7048
	TiW	31.30 ± 1.35	29.6 ± 1.3	<0.05
	TiSR	14.14 ± 1.33	26.1 ± 4.0	<0.05
	MTiTH	41.75 ± 4.08	42.0 ± 5.1	0.8434
	MalW	62.69 ± 2.86	63.1 ± 3.4	0.6304
	APA(deg)	26.34 ± 5.09	7.4 ± 5.7.0	<0.05
	MLATi(deg)	5.88 ± 2.49	12.5 ± 3.0	<0.05
Talus	TaAL	31.42 ± 1.63	32.3 ± 4.1	0.3545
	TaWc	27.33 ± 1.23	20.9 ± 3.0	<0.05
	TaWa	27.18 ± 2.13	26.8 ± 4.0	0.6871
	TaWp	24.03 ± 1.25	14.3 ± 3.4	<0.05
	TaRl	16.77 ± 0.91	20.8 ± 3.0	<0.05
	TaRn	10.31 ± 0.71	20.8 ± 3.0	<0.05
	TaRm	12.27 ± 0.75	21.8 ± 3.0	<0.05
	TaH	14.58 ± 1.59	11.9 ± 1.8	<0.05
	TaIA(deg)	4.08 ± 2.39	12.9 ± 6.7	<0.05
	MLATa(deg)	8.06 ± 3.71	1.1 ± 1.1	<0.05

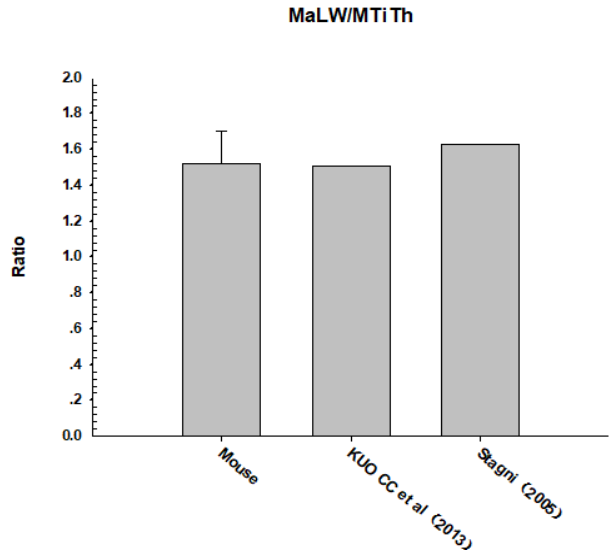

Figure 4. Mean ratios of the anteroposterior (thickness) and mediolateral (width)dimensions of (MalW/MTiTH) values across all specimens in the current study (error bar: 95% CI), and the same dimensions reported in Stagni and Kuo's study.

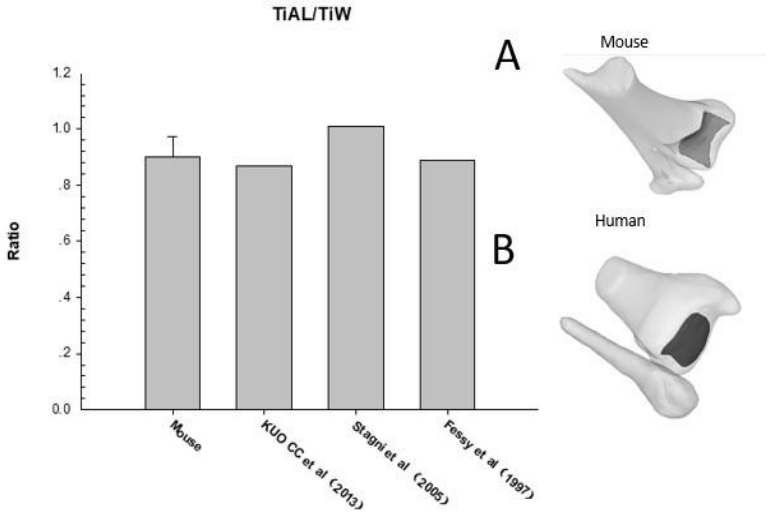

Figure 5. Mean ratios of the anteroposterior (thickness) and mediolateral (width) dimensions of tibial mortise (TiAL/TiW) in the mouse (A), human (B) and the trochlea tali (TaAL/TaW).

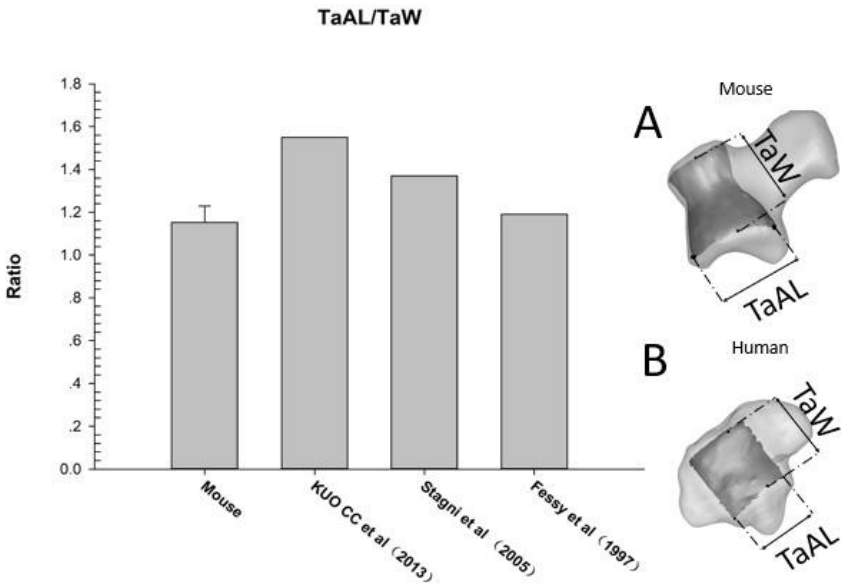

Figure 6. Across all specimens in the current study (95% CI), and the ratios of the means of the same dimensions reported in published literature.

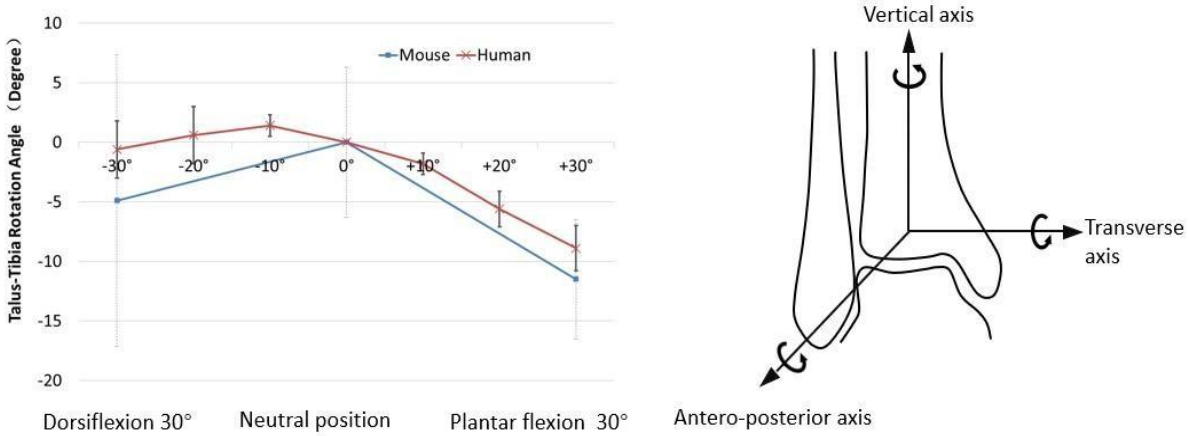

Figure 7. The rotational displacement of the talus around the tibial axis compared with the neutral position (positive difference between values denotes internal rotation around the vertical tibial axis).

4. Discussion

Structure governs function. The ankle, or talocrural joint, is a synovial hinge joint that connects the distal ends of the tibia and fibula with the proximal end of the talus. It is the only mortise and tenon joint in human body. Investigating the skeletal morphometry of the mouse and assessing its similarities and differences with the human is particularly important when considering the simulation of an ankle sprain. However, the relevant parameters of the mouse ankle joint bones are particularly scarce [24]. The purpose of this study was to determine the morphometric parameters of ankle joints based on high-resolution micro-CT images. This study

highlighted the underlying potential of isotropic micro-CT image data for comparing complex surface topographies of the ankle in the mouse and human. Previous studies of the skeletal anatomy of the mouse hindfoot have generally focused on the gross anatomy of the hindlimb [24,25] or the magnitude of the muscle moment arm [26], instead of detailed geometry of the ankle joint. The musculoskeletal geometry of ankle joints has not yet been comprehensively investigated. Prior to comparing human and mouse data, normalization is essential. During our analysis, it was found that the ratio between MalW and MTiTH in the mouse was similar to that in humans. Thus, the MalW/ MTiTH ratio was deemed reliable for normalization purposes.

4.1. Morphological Size, Angle and Kinematics

When comparing the size data acquired herein, it was found that the mean normalized malleolar width, tibial thickness, tibial arc length, trochlea tali arc length and trochlea tali width of anterior talus parameters were similar to those measured in humans. The ratio of malleolar width (MalW) to tibial width (TiW) for the mouse and humans is similar, indicating that the talocrural joint of both the tibia and talus share the same general mortise bony architecture. The radii of the tibia and talar dome of the mouse was smaller than those in the human in the sagittal plane, indicating that the curvature of talar dome was tighter than in humans. The ratio of TiSR: TiAL was 0.5 in the mouse and 0.9 in the human, indicating that the human distal tibia could cover a larger part of the talar dome. The mouse ankle is more like a ball- and socket joint, while the human ankle is more similar to a rectangular socket joint. The tibial width, the center and posterior crests of the talar dome width and the talar head height were larger than those of a human, suggesting that the talar dome was covered more by the tibia. The mouse has a thicker trochlea tali, allowing greater stability in the mouse ankle joint. In addition, the talar dome in the mouse has a groove, the lateral side of trochlea tali radius (TaR) of the talar dome is 36.6% larger than the medial side and the narrowest radius is in the middle of the talar dome, which is 84.0% of the medial side and 61.4% of the lateral side, respectively. For the angle data, the MLATi value in the mouse was smaller than in the human, indicating that the inferior tibiofibular joint of a mouse has a lower distal fibular position than in a human, suggesting that the mortise and tenon joint could be more stable. The APA in the mouse was larger than that in a human, indicating that the distal tibia covers the talar dome by more spectrum. The MLATa in mice was larger than that in humans, indicating that the mouse has a higher talar dome on the lateral side than the medial side. In the human joint, the talus rotated −0.6° and −8.9 ° in 30 °dorsiflexion and 30 ° plantarflexion, while the rotation was −4.89 °and −11.49 ° in the mouse. The vertical rotation of the mouse talus tended in the same direction as that of the human but was of a larger magnitude [22].

4.2. Skeletal Comparison among Animals

In a previous study by Turner et al [11], mouse ankle joints were used to simulate human ankle injury. Animal models are more credible than cadaveric or computer models. Because animal models can observe the effects of damage over a long duration, they are dynamic and more in line with the pathological process of human ankle sprains. Up to now only animal models have been used in the study of the functional mechanisms of the ankle. Thus, animal models can provide a better perspective for studying ankle sprains. Instability and injury are established in the mouse

and rat, and not in other common animals. Although chimpanzees are closely-related to humans, their foot function is regarded more like a hand because they live in trees most of the time [27]. The calcaneus in the cow and dog do not even touch the ground, as they use the metatarsal-phalangeal joint more for walking and running. Rabbits have an ankle joint similar to humans, while the distal tibia and fibula are fused. However, rabbits would prefer to remain stationary most of time rather than run around, and this behavior is not suitable for gait analysis. Therefore, rodents such as the rat or mouse are the most appropriate animal model for the study of ankle injury because of the gross similarity of the ankle joint to humans and features for motion analysis in an experimental situation. However, in a previous study, the majority of the experiments were performed using mice. The rats and mice had no significant abnormalities in the ankle anatomy except for the difference in anatomical size. Future studies should study rats to investigate whether there is a difference between rat and mouse anatomy. The ankle joint is very important in the study of the relationship between morphology and function, as it is a major contributor to all rotations of the foot and transmits all forces encountered from the foot to the leg [28].

4.3. Foot and Subtalar Joint vs Ankle Joint

In this study, based on a 3D skeletal model of the foot and ankle, we can see that the mouse foot is much slimmer than the human, while the proportions of the ankle joint are similar. Furthermore, mice have flat feet without a prominent longitudinal arch. The calcaneus bone is substantially longer than that of a human, which can provide a longer moment arm for propulsive force during locomotion [29]. The shapes of the talus and tibia explain the ability of a mouse to achieve a large ankle dorsiflexion and it also provides the ability for the foot to conform to various substrates during vertical climbing [30]. The subtalar joint functions as a plane synovial joint, which is the principal site within the foot for achieving eversion and inversion movements.

4.4. Two-dimensional vs Three-dimensional

Three-dimensional imaging techniques have become popular in clinical and scientific research. Huang's study [31] used three-dimensional imaging to analyze B-scans. In this study, we use this technique to analyze micro-CT scans. To date, ankle morphometry has been assessed using plain radiographic measurements. Radiographs can be useful for studies of the structure of the hindfoot. However, it does not allow true estimation of ankle 3D morphology, and differences in posture and tube projection angles may cause substantial variability in structural variables. Conversely, CT images of the foot and ankle were relatively consistent. Although CT images are two-dimensional, CT data can be used to construct 3Dcomputer-assisted models, which provide substantially more information regarding the morphology of the talus. For example, because the talar dome is wedge-shaped in the transverse plane (wider anteriorly than posteriorly on the superior surface), the maximum value would most likely be measured radiographically in a mortise view plane. In addition, the intrinsic error on plain radiographic measurement is very sensitive to ankle positioning. Technological advances in high-resolution micro-CT [32] now permit isotropic 3D evaluation of bone morphometry. Inconclusion, the morphometric data reported in this study comprehensively described the topographical features of the mouse ankle joint.

5. Conclusion

There is a certain similarity in the ankle of the mouse and human, but it also has some differences. Because previous studies [11] have used mice to simulate human ankle joints, this paper focuses on the similarities between the two. In the previous section, we discussed the anatomy of the ankle of several animals and finally found that mice are most suitable for simulating human ankle joints. This suggests that mice have more similar ankle anatomy to humans than other experimental animals. The mouse ankle was a close analogue to that of a human. Gross skeletal similarity in the mouse and human talocrural joint features was observed, including malleolar width and thickness, and trochlea tali arc length and width. Structure governs function, the mouse talus had a larger curvature of arc radius and an uneven double-drum asymmetric talar dome structure, which provides better stability than that in humans. This study provided valuable information and insight into the control of the musculoskeletal system in humans. The mouse ankle mimics the mechanisms to a large extent of human ankle functioning and thus, the mouse could be an appropriate animal model for better understanding of ankle biomechanics in general. However, the differences in the talar dome in the mouse and human based on their anatomical skeletal differences should also be noted.

Limitations

Firstly, although the thickness of the cartilage was not included in the measurements, the technique utilized is likely to be useful in assessing similarities in ankle morphology. In the present study, prior to making measurements of each specimen, a local coordinate system was established using bony landmarks as a reference. This anatomical coordinate system allowed characterization of ankle morphological features. Determination of the coordinate system included visual identification of landmarks, which could affect reproducibility. Fortunately, slight differences in the coordinate system positioning actually had a minimal effect on measurements [15]. Secondly, there is variation among the mouse strains in anatomical features of the tarsals, according to previous studies. We utilized statistics that were based on the C57BL/6mouse strain in this study. Since we only explored the bony structure in the present study, we will investigate the ligament in a future study. Here, we mainly focused on morphological measurements of the ankle joint, i.e. the talus, with adjacent bones such as the navicular and calcaneus not being involved. We are planning further investigations on other adjacent bones in future work. The degree of varus and valgus of the ankle joint is closely related to ankle sprain. However, due to the fixed mold in this study, the ankle joint could only perform dorsiflexion and plantarflexion in the sagittal plane, so its range of varus and valgus could not be measured. We will pay attention to this limitation in future experiments and make further measurements.

Acknowledgments

This work was supported by the National Key R&D Program of China (No. 2018YFB1107000), National Natural Science Foundation of China (11572211, 31270995, 31771063, 31570978), Jiangsu Provincial Commission of Health and Family Planning (H201619), and the Priority Academic Program Development of Jiangsu Higher Education Institutions (PAPD).

Conflict of interest

All authors declare no conflicts of interest in this paper

References

1. X. Li, D. Fong and K. M. Chan, Kinematic analysis of ankle eversion sprain in sports: two cases during the FIFA world cup, *J. Orthop. Transl.*, **7** (2016), 135.
2. J. M. Conn, J. L. Annest and J. Gilchrist, Sports and recreation related injury episodes in the US population, 1997-99, *Inj. Prev.*, **9** (2003), 117.
3. B. R. Waterman, B. D. Owens, S. Davey, et al., The epidemiology of ankle sprains in the United States., *J. Bone Joint Surg. Am.*, **92** (2010), 2279.
4. W. Niu, J. Yao, Z. W. Chu, et al., Effects of Ankle Eversion, Limb Laterality, and Ankle Stabilizers on Transient Postural Stability During Unipedal Standing, *J. Med. Biol. Eng.*, **35** (2015), 69–75.
5. R. Bahr, F. Pena, J. Shine, et al., Mechanics of the anterior drawer and talar tilt tests. A cadaveric study of lateral ligament injuries of the ankle, *Acta Orthop. Scand.*, **68** (1997), 435.
6. C. M. Gorehamvoss, T. O. Mckinley and T. D. Brown, A finite element exploration of cartilage stress near an articular incongruity during unstable motion, *J. Biomech.*, **40** (2007), 3438–3447.
7. F. Bonnel, E. Toullec and C. Mabit, Chronic ankle instability: Biomechanics and pathomechanics of ligaments injury and associated lesions, *Orthop. Traumatol. Surg. Res.*, **96** (2010), 424–432.
8. H. Fang and F. Beier, Mouse models of osteoarthritis: modelling risk factors and assessing outcomes, *Nat. Rev. Rheumatol.*, **10** (2014), 413–421.
9. K. Lampropoulouadamidou, P. Lelovas, E. V. Karadimas, et al., Papaioannou, Useful animal models for the research of osteoarthritis, *Eur. J. Orthop. Surg. Traumatol.*, **24** (2014), 263–271.
10. P. Fleckman, K. Jaeger, K. A. Silva, et al., Comparative anatomy of mouse and human nail units, *Anat. Rec.*, **296** (2013), 521–532.
11. T. Hubbard-Turner, E. A. Wikstrom, S. Guderian, et al., Acute ankle sprain in a mouse model, *Med. Sci. Sports Exerc.*, **45** (2013), 1623–1628.
12. S. H. Chang, T. Yasui, S. Taketomi, et al., Comparison of mouse and human ankles and establishment of mouse ankle osteoarthritis models by surgically-induced instability, *Osteoarth. Cartil.*, **24** (2015), 688–697.
13. H. Y. Kim, J. Wang, K. Chung, et al., A surgical ankle sprain pain model in the rat: Effects of morphine and indomethacin, *Neurosci. Lett.*, **442** (2008),161–164.
14. E. A. Wikstrom, T. Hubbardturner, S. Woods, et al., Developing a mouse model of chronic ankle instability, *Med. Sci. Sports Exerc.*, **47** (2015), 866–872.
15. A. Hayes, Y. Tochigi and C. L. Saltzman, Ankle morphometry on 3D-CT images, *Iowa Orthop. J.*, **26** (2006), 1–4.
16. K. I. Vadakkan, Y. H. Jia and M. Zhuo, A behavioral model of neuropathic pain induced by ligation of the common peroneal nerve in mice., *J. Pain*, **6** (2005), 747–756.
17. M. H. Fessy, J. P. Carret and J. B ĝui, Morphometry of the talocrural joint, *Surg. Radiol. Anat.*, **19** (1997), 299–302.
18. R. Stagni, A. Leardini, A. Ensini, et al., Ankle morphometry evaluated using a new semi-automated technique based on X-ray pictures, *Clin. Biomech.*, **20** (2005), 307–311.

19. W. D. Hazelton, G. Goodman, W. N. Rom, et al., Longitudinal multistage model for lung cancer incidence, mortality, and CT detected indolent and aggressive cancers, *Math. Biosci.*, **240** (2012), 20–34.
20. S. P. Chakrabarty, F. B. Hanson, Distributed parameters deterministic model for treatment of brain tumors using Galerkin finite element method, *Math. Biosci.*, **219** (2009),129–141.
21. C. C. Kuo, H. L. Lu, A. Leardini, et al., Three-dimensional computer graphics-based ankle morphometry with computerized tomography for total ankle replacement design and positioning, *Clin. Anat.*, **27** (2014), 659.
22. A. Lundberg, I. Goldie, B. Kalin, et al., Kinematics of the ankle/foot complex: plantarflexion and dorsiflexion, *Foot Ankle*, **9** (1989), 194.
23. J. Yu, W. C. Wong, H. Zhang, et al., The influence of high-heeled shoes on strain and tension force of the anterior talofibular ligament and plantar fascia during balanced standing and walking, *Med. Eng. Phys.*, **38** (2016), 1152–1156.
24. J. P. Charles, O. Cappellari, A. J. Spence, et al., Musculoskeletal geometry, muscle architecture and functional specialisations of the mouse hindlimb, *PLOS ONE*, **11** (2016), e147669.
25. A. Delaurier, N. Burton, M. Bennett, et al., The Mouse Limb Anatomy Atlas: an interactive 3D tool for studying embryonic limb patterning, *BMC Dev. Biol.*, **8** (2008), 83.
26. W. L. Johnson, D. L. Jindrich, R. R. Roy, et al., A three-dimensional model of the rat hindlimb: musculoskeletal geometry and muscle moment arms, *J. Biomech.*, **41** (2008), 610–619.
27. T. R. Olson and M. R. Seidel, The evolutionary basis of some clinical disorders of the human foot: a comparative survey of the living primates, *Foot Ankle*, **3** (1983), 322.
28. W. C. H. Parr, C. Soligo, J. Smaers, et al., Three-dimensional shape variation of talar surface morphology in hominoid primates, *J. Anat.*, **225** (2014), 42–59.
29. S. Duce, L. Madrigal, K. Schmidt, et al., Micro-magnetic resonance imaging and embryological analysis of wild-type and pma mutant mice with clubfoot, *J. Anat.*, **216** (2010), 108.
30. D. Youlatos and J. Meldrum, Locomotor diversification in new world monkeys: running, climbing, or clawing along evolutionary branches, *Anat. Rec.*, **294** (2011), 1991–2012.
31. Q. Huang, X. Huang, L. Liu, et al., A case-oriented web-based training system for breast cancer diagnosis, *Comput. Meth. Prog. Bio*.
32. V. Kuhn, N. Ivanovic and W. Recheis, High resolution 3D-printing of trabecular bone based on micro-CT data, *J. Orthop. Transl.*, **2** (2014), 238.